Research Square

Preprints are preliminary reports that have not undergone peer review.
They should not be considered conclusive, used to inform clinical practice,
or referenced by the media as validated information.

Single-cell and spatial multi-omics reveal inter-focal heterogeneity yet convergent immunosuppressive programs in multifocal hepatocellular carcinoma

Cheng Wu
Guangzhou Medical University
Ke Si
Guangzhou Medical University
Shuai Mao
The First Affiliated Hospital, Sun Yat-sen University
Zehang Jiang
Guangzhou Medical University
Douyue Li
Guangzhou Medical University
Haipeng Zhu
First Affiliated Hospital of Guangzhou Medical University
Ningning Sun
First Affiliated Hospital of Guangzhou Medical University
Weiling Liang
University of Hong Kong - Shenzhen Hospital
Wenliang Zhang
zhangwl25@alumni.sysu.edu.cn

Guangzhou Medical University

Research Article

Keywords: Multifocal hepatocellular carcinoma, Inter-focal heterogeneity, Single-cell multi-omics, Immunosuppressive microenvironment, TMED2–ADAR1–C3/C5 axis

Posted Date: October 15th, 2026

DOI: https://doi.org/10.21203/rs.3.rs-11111917/v1

License: This work is licensed under a Creative Commons Attribution 4.0 International License.
Read Full License

Additional Declarations: No competing interests reported.

Single-cell and spatial multi-omics reveal inter-focal heterogeneity yet convergent immunosuppressive programs in multifocal hepatocellular carcinoma

Cheng Wu[1†], Ke Si[1†], Shuai Mao[2†], Zehang Jiang[1†], Douyue Li[1], Haipeng Zhu[1,3], Ningning Sun[1,3], Weiling Liang[4], Wenliang Zhang[1,3,4*]

[1] The Key Laboratory of Advanced Interdisciplinary Studies, The First Affiliated Hospital of Guangzhou Medical University, GMU-GIBH Joint School of Life Sciences, The Guangdong-Hong Kong-Macao Joint Laboratory for Cell Fate Regulation and Diseases, Guangzhou Medical University, Guangzhou 510182, People's Republic of China;

[2] Department of Pancreato-Biliary Surgery, the First Affiliated Hospital, Sun Yat-sen University, Guangzhou, 510080, China;

[3] Department of Hepatobiliary Surgery, The First Affiliated Hospital of Guangzhou Medical University, Guangzhou 510120, People's Republic of China;

[4] Department of Pediatrics, The University of Hong Kong-Shen Zhen Hospital, Shenzhen 518053, People's Republic of China.

[†] These authors contributed equally.

[*]Corresponding author:

Professor Wenliang Zhang, Ph.D, The Key Laboratory of Advanced Interdisciplinary Studies, The First Affiliated Hospital of Guangzhou Medical University, GMU-GIBH Joint School of Life Sciences, The Guangdong-Hong Kong-Macao Joint Laboratory for Cell Fate Regulation and Diseases, Guangzhou Medical University, Guangzhou 510182, People's Republic of China; Email: zhangwl25@alumni.sysu.edu.cn. ORCID: 0000-0003-0454-6935

Short title: Convergent immunosuppressive programs in multifocal HCC

Abstract

Background Multifocal hepatocellular carcinoma (HCC) comprises separated tumor foci with divergent evolutionary trajectories, raising the clinical question of whether strategies should target lesion-specific vulnerabilities or shared dependencies across heterogeneous lesions. We aimed to resolve inter-focal malignant and microenvironmental heterogeneity and define convergent immunosuppressive programs that may represent shared therapeutic vulnerabilities across multifocal HCC.

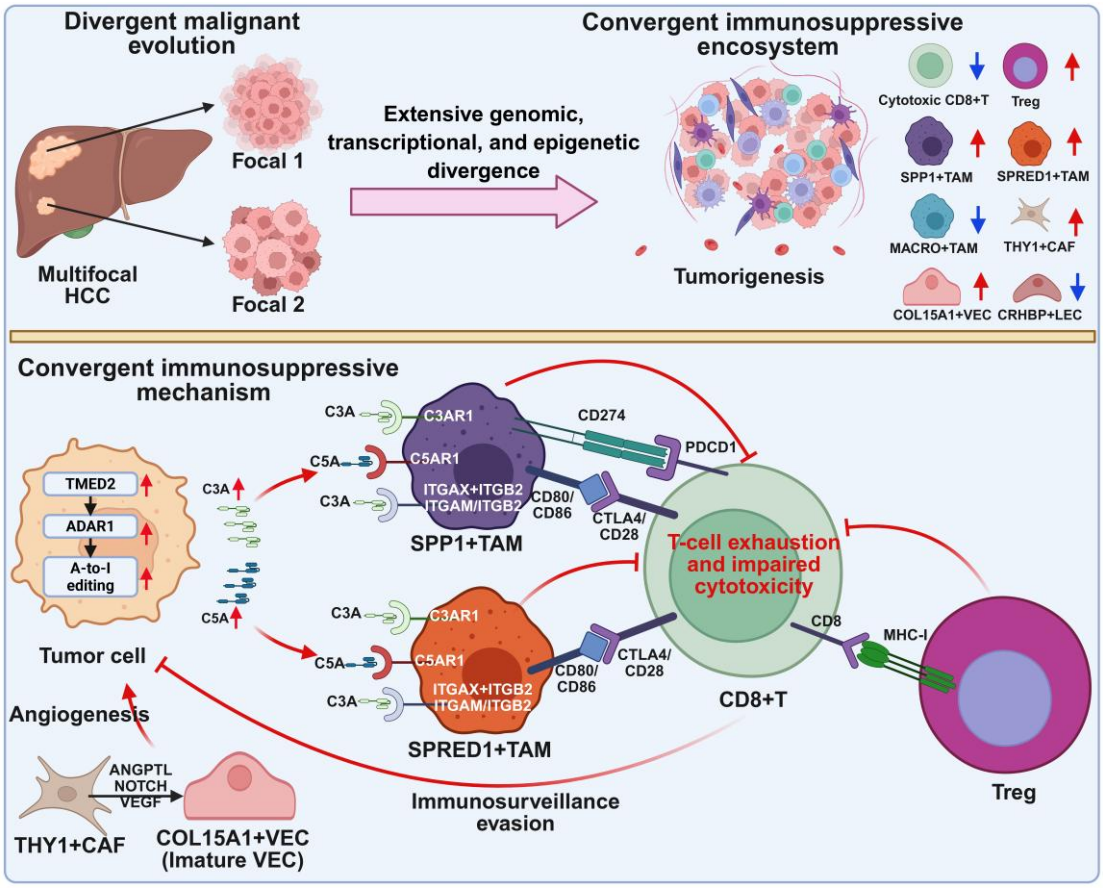
Methods We obtained 18 spatially distinct tissue samples from five patients with multifocal HCC, including different tumor lesions, paired adjacent non-tumor tissues, and normal liver tissues. Samples were profiled by scFAST-seq (15 samples), scATAC-seq (12 samples), and Stereo-seq (12 samples) for integrated single-cell, epigenomic, and spatial multi-omic analysis. In-house RNA-seq, public scRNA-seq (HRA001748, 88 samples) and RNA-seq datasets (TCGA-LIHC, OEP000321) were used for validation. We performed multiplex immunohistochemistry on 48 paired multifocal hepatocellular carcinoma and adjacent non-tumor tissues, complemented by functional assays to validate key findings.

Results Multifocal HCC exhibited extensive inter-focal heterogeneity in malignant genomic, transcriptional, epigenetic, and evolutionary states, accompanied by diverse immune and stromal landscapes. Despite this divergence, spatially separated tumor foci converged on shared malignant states marked by elevated *TMED2* expression and convergent immunosuppressive ecosystems characterized by regulatory T-cell (Treg) and SPP1+/SPRED1+ macrophage enrichment, impaired cytotoxic CD8+ T-cell immunity, and recurrent stromal–vascular remodeling. Mechanistically, malignant hepatocytes engaged SPP1+/SPRED1+ macrophages through C3/C5 complement signaling across divergent tumor foci, while macrophages and Tregs contributed to CD8+ T-cell dysfunction through CD274–PDCD1,

CD80/CD86–CTLA4/CD28, and MHC-I–CD8 interactions. A tumor-intrinsic TMED2–ADAR1-dependent A-to-I RNA editing program promoted C3/C5 complement expression and secretion, linking malignant heterogeneity to convergent tumor–immune signaling.

Conclusion Despite divergent malignant evolution, multifocal HCC converges on shared immunosuppressive ecosystems. The TMED2–ADAR1–C3/C5 complement axis represents a conserved tumor–immune vulnerability that may enable therapeutic strategies targeting common immune-evasion mechanisms across heterogeneous tumor foci.

Key Words: Multifocal hepatocellular carcinoma; Inter-focal heterogeneity; Single-cell multi-omics; Immunosuppressive microenvironment; TMED2–ADAR1–C3/C5 axis



Graphic abstract

Introduction

Hepatocellular carcinoma (HCC) remains one of the leading causes of cancer-related mortality worldwide[1]. Approximately 35–50% of patients present with multifocal disease at diagnosis[2, 3], which is associated with increased recurrence, therapeutic resistance, and poor survival compared with unifocal tumors[4]. Multifocal HCC provides a unique clinical model to investigate how malignant evolution influences tumor microenvironment organization. Spatially separated tumor foci may arise through intrahepatic metastasis (IM), reflecting clonal dissemination from an ancestral tumor, or multicentric occurrence (MO), resulting from independent tumorigenic events in chronically injured liver tissue[5]. Such distinct evolutionary origins provide an opportunity to investigate how divergent malignant evolution shapes the cellular and molecular landscape of individual tumor foci and, importantly, whether distinct malignant states retain shared mechanisms of immune evasion.

Recent genomic and multi-omic studies have revealed extensive molecular diversity among spatially separated HCC lesions from the same patient. Whole-genome sequencing has uncovered distinct clonal architectures and mutational landscapes distinguishing IM and MO lesions[5], while integrative analyses have identified inter-focal differences in HBV integration patterns, copy-number alterations, structural variants and driver alterations[6, 7]. Beyond genomic alterations, transcriptomic[8], immunogenomic[9], proteogenomic[10], and microbiome[11] studies have further revealed differences in malignant cell states, metabolic programs, immune landscapes, microbe–host interactions, and ecological niches across tumor foci. Single-cell RNA-seq studies have provided additional evidence of heterogeneous cellular states and immune compositions across IM and MO lesions[12]. Collectively, these studies establish substantial molecular and cellular heterogeneity across tumor foci, but the cellular and spatial

mechanisms underlying this heterogeneity remain poorly resolved, particularly how divergent malignant populations interact with surrounding immune and stromal compartments.

Tumor evolution is traditionally viewed as a process in which progressive genetic and epigenetic diversification generates increasingly heterogeneous malignant populations[13]. Yet malignant cells evolve within complex tumor ecosystems in which immune, stromal, and vascular compartments both impose selective pressures and respond to tumor-derived signals[14, 15]. Therefore, divergent evolution may generate distinct malignant states without necessarily producing distinct mechanisms of immune escape. Evolutionarily separated tumor foci may retain convergent tumor–immune interactions that sustain immune evasion despite molecular divergence. Whether such evolutionary convergence of immune suppression exists across multifocal HCC remains largely unknown.

Defining such convergent immune-evasion programs is clinically important because lesion-specific alterations may limit the durability of therapies targeting individual malignant clones. Identifying vulnerabilities shared across distinct tumor foci could enable therapeutic strategies that overcome inter-focal heterogeneity. Here, we integrated cutting-edge single-cell and spatial multi-omics approaches to resolve malignant evolution, cellular states, spatial organization, and tumor–immune interactions across multifocal HCC. This integrated approach revealed extensive inter-focal divergence alongside conserved immunosuppressive signaling, providing a framework to distinguish shared functional dependencies from lesion-specific cellular states and to identify potential therapeutic vulnerabilities across multifocal disease.

Methods

Patient cohort and study design

All patients with primary multifocal HCC were enrolled in this study. All patients were newly diagnosed, harbored at least two anatomically distinct tumor foci, and had received no anticancer treatment before surgical resection. Hepatitis virus infection was not used as an inclusion or exclusion criterion. Each tumor focus and its matched adjacent non-tumor liver tissue were collected separately during surgery. Detailed clinicopathological characteristics of the patients are provided in **Supplementary Fig. 1 and Table S1,2**.

Integrated single-cell and spatial multi-omics profiling was performed on 18 spatially distinct tissue samples from five patients with multifocal HCC, including scFAST-seq (15 tumor/adjacent tissue samples), scATAC-seq (12 samples), and Stereo-seq (12 samples). For independent validation, a tissue microarray comprising 48 paired multifocal HCC tumor foci and matched adjacent liver tissues (**Supplementary Table S3**) was constructed by Bioaitech Co., Ltd. (China), and bulk RNA sequencing was performed on 13 samples from 10 patients (**Supplementary Table S2**).

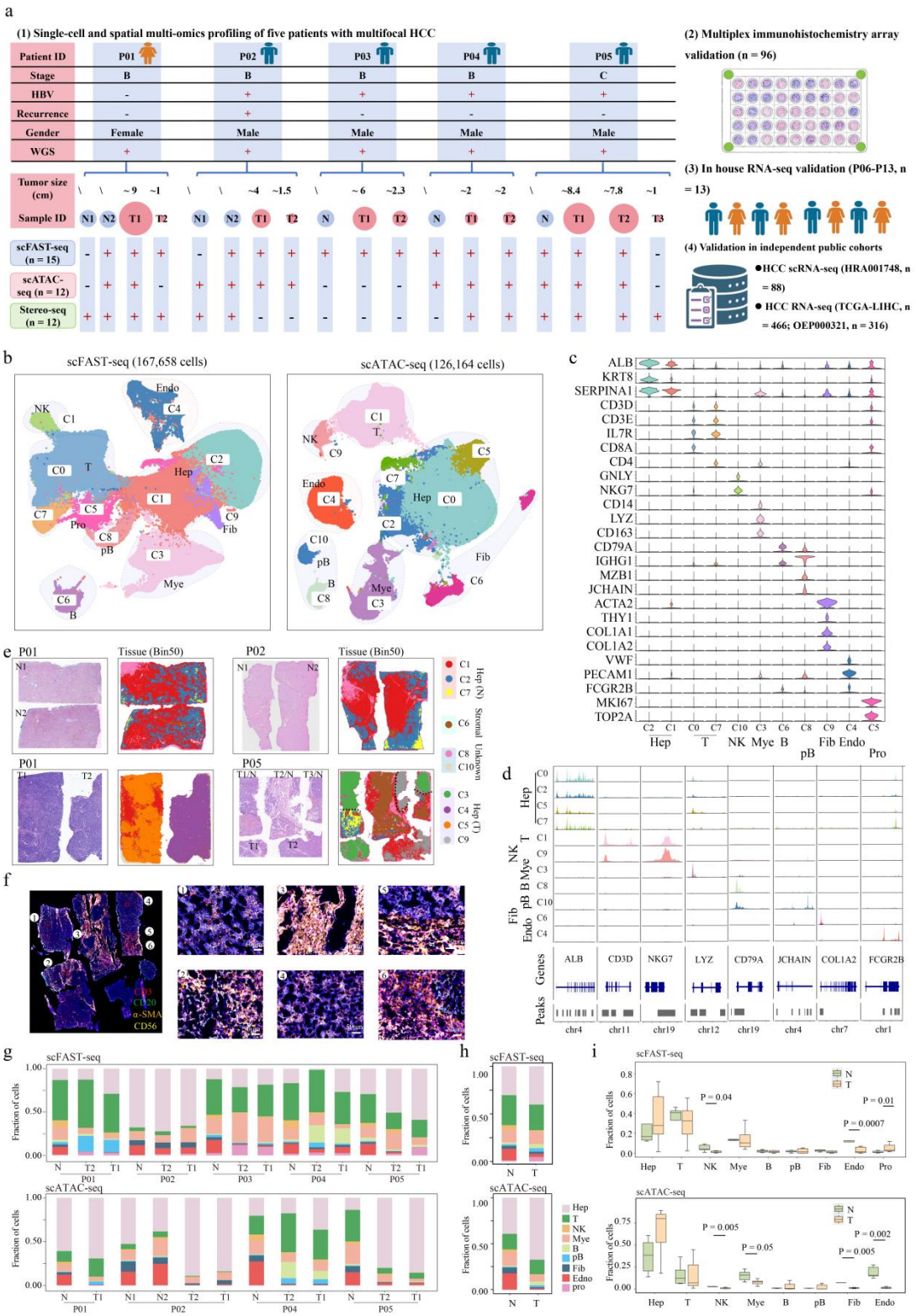
To further validate these findings, we integrated large-scale public datasets, including scRNA-seq data from HRA001748 cohort (n = 88)[16] and bulk RNA-seq from TCGA-LIHC (n = 466, UCSC Xena, https://xena.ucsc.edu/) and OEP000321 (n = 316)[17]. Further functional validation, including gene perturbation, proliferation, migration, ELISA, and qPCR assays, was conducted to investigate the identified molecular mechanisms. All patients provided written informed consent, and the study was approved by the Ethics Committee of Guangzhou Medical University (approval no. 202405020). For further details regarding the materials and

methods, please refer to the **supplementary information** and the **Supplementary Tables S1-S7**.

Results

Single-cell and spatial multi-omics define the cellular and spatial landscape of multifocal HCC

To characterize the cellular and spatial landscape across tumor foci in multifocal HCC, we performed integrated single-cell and spatial multi-omic profiling of matched tumor and peritumoral tissues (**Fig. 1a)**. scFAST-seq generated 167,658 high-quality single cells and resolved nine major cell populations, including hepatocytes (Hep), T cells, NK cells, myeloid cells (Mye), B cells, plasma cells (pB), fibroblasts (Fib), endothelial cells (Endo), and proliferating cells (Pro) (**Fig. 1b,c**). Complementary scATAC-seq profiling of 126,164 nuclei identified eight chromatin-accessibility-defined cell populations, which showed consistent annotation with transcriptomic profiles (**Fig. 1b,d**). Integrated analyses demonstrated high concordance across samples with minimal batch effects (**Supplementary Fig. 2a**), supporting the robustness of the multi-omic dataset.



[**Fig. 1 Integrated single-cell and spatial profiling of multifocal HCC. (a)** Overview of the study design. **(b)** UMAP plot of cell lineages from scFAST-seq (left) and scATAC-seq (right) in multifocal HCC. **(c,d)** Violin plots showing marker gene expression across cell types in scFAST-seq **(c)** and scATAC-seq

(d). **(e)** H&E images and spatial cell-type annotation of representative adjacent normal (N) and tumor (T) tissues. **(f)** Multiplex immunohistochemistry validation of major cell populations and spatial organization of patient P05. **(g)** Stacked bar plots showing cell-type proportions across tumor foci from individual patients and between adjacent normal (N) and tumor (T) tissues. **(h)** Comparison of major cell-type proportions between adjacent normal (N) and tumor (T) tissues.]

Spatial transcriptomic profiling using Stereo-seq further mapped cellular organization within tumor tissues and provided spatial context for heterogeneous tumor ecosystems (**Fig. 1e**). H&E staining distinguished tumor, adjacent normal, and stromal regions, enabling spatial interpretation of molecular patterns (**Fig. 1e, Supplementary Fig. 2b**). Spatial clustering identified 14 distinct cell clusters representing diverse cellular states, including non-malignant hepatocytes (C1, C2, and C7, predominantly from P01_N1/N2 and P02_N1/N2), malignant hepatocytes (C3 mainly from P04_T2 and P05_T1/T3; C4 and C5 primarily from P01_T1/T2; C9 mostly from P05_T2), and stromal/immune-enriched regions (C6) (**Fig. 1e, Supplementary Fig. 2b**). Non-malignant hepatocytes exhibited *ALB* expression, whereas malignant hepatocyte regions displayed elevated *GPC3* expression. Immune and stromal regions were characterized by *CD3D*, *CD14*, and *ACTA2* expression, respectively (**Supplementary Fig. 2c,d**). These spatial assignments were further validated by mIHC (**Fig. 1f**).

Comparative analysis of cellular composition revealed extensive inter-focal heterogeneity among tumor lesions and matched peritumoral tissues (**Fig. 1g**). Notably, scATAC-seq showed higher hepatocyte representation than scFAST-seq, likely reflecting differences in cellular fragility and nuclear accessibility during sample processing (**Fig. 1g, Supplementary Fig. 2e**). Smaller tumor foci (e.g., P01_T2, P04_T2) exhibited increased T-cell infiltration compared with their corresponding larger lesions (P01_T1, P04_T1)

(**Fig. 1g**), consistent with spatial observations from Stereo-seq (**Supplementary Fig. 2f**). Furthermore, HBV-associated, recurrent, and advanced-stage tumors displayed increased hepatocyte abundance accompanied by reduced T-cell infiltration, suggesting differential immune remodeling among tumor foci (**Supplementary Fig. 2g**).

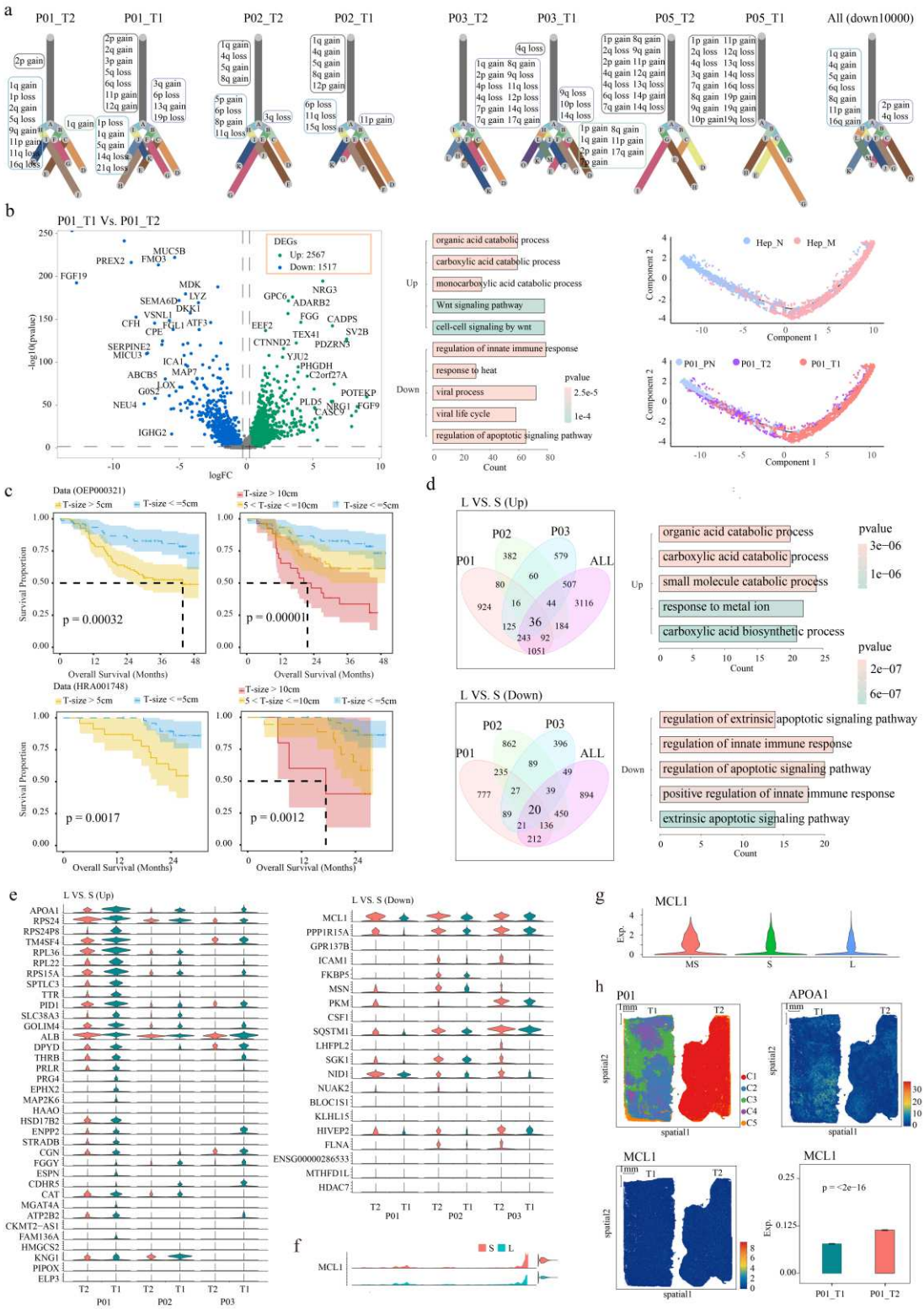
Across the cohort, tumor foci were characterized by expansion of malignant hepatocyte and proliferative populations together with depletion of immune and stromal compartments compared with peritumoral tissues (**Fig. 1g,h**). This immune-desert phenotype was further supported by independent public single-cell HCC datasets (**Supplementary Fig. 3a–d**). Collectively, these findings demonstrate marked inter-focal heterogeneity alongside conserved malignant and tumor microenvironmental remodeling across multifocal HCC.

Divergent evolutionary trajectories generate heterogeneous yet conserved malignant states in multifocal HCC

To define the evolutionary basis of inter-focal heterogeneity, we reconstructed clonal trajectories of malignant hepatocytes across paired tumor foci using large-scale CNV inference. We observed a tendency for tumor foci with marked differences in size to be associated with intrahepatic clonal expansion, whereas lesions of comparable size tended to occur in cases with multicentric origins (**Fig. 2a**). Accordingly, in P01, P02 and P03, the smaller T2 lesions appeared to arise through clonal expansion from the larger T1 lesions, whereas P05_T1 and P05_T2 harboured distinct CNV patterns consistent with independent clonal evolution (**Fig. 2a**). Due to limited residual tissue availability after multi-omics profiling, WGS-based somatic mutation phylogenetic analysis could not be performed across all tumor foci. Therefore, these inferred relationships represent putative evolutionary patterns rather

than definitive classifications of intrahepatic metastasis or multicentric occurrence.

Pseudotime and transcriptional pathway analyses further supported these evolutionary patterns, with smaller T2 lesions in P01, P02 and P03 occupying intermediate differentiation states, whereas P05 lesions followed distinct trajectories consistent with multicentric origins (**Fig. 2b, Supplementary Fig. 4a–f**). Despite these differences in lesion formation, larger T1 lesions consistently exhibited enhanced catabolic, biosynthetic and proliferation-related signalling compared with smaller T2 lesions, alongside suppressed immune, antiviral and apoptotic programmes, consistent with progressive metabolic adaptation and immune evasion (**Fig. 2b, Supplementary Fig. 4a–f**). Consistent with these findings, larger lesions were associated with poorer survival and showed enhanced metabolic and biosynthetic activity together with reduced apoptotic and innate immune programmes, accompanied by concordant changes in chromatin accessibility and validated in public HCC datasets (**Fig. 2c–e, Supplementary Fig. 5a–c**). Integrated transcriptomic and epigenetic analyses further identified lesion size progression-associated genes with coordinated regulatory changes, including *MCL1* and *APOA1* (**Fig. 2f–h, Supplementary Fig. 5d–f**).

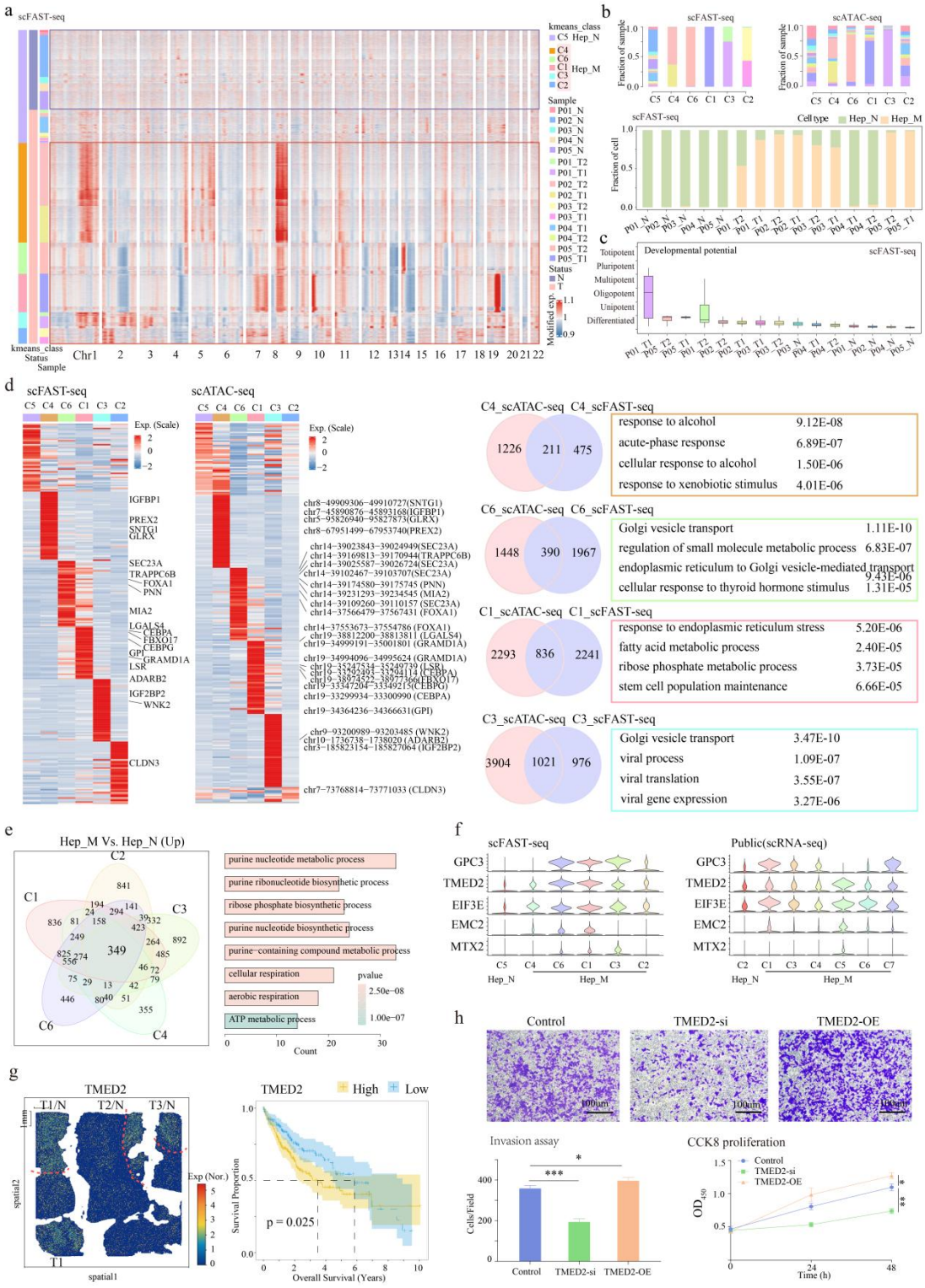


[**Fig. 2 Clonal evolution and size-associated malignant reprogramming across tumor foci in multifocal HCC. (a)** Clonality trees for each tumor focus from P01, P02, P03, P05, with branch lengths representing the number of cells in each subclone. Chromosomal gains and losses were inferred to

reconstruct the clonal evolution. P04 was excluded from the clonality tree analysis due to insufficient malignant hepatocytes in both P04_T1 and P04_T2 for reliable inferCNV-based clonal reconstruction, as reflected by the low malignant cell representation. **(b)** Volcano plot showing differentially expressed genes between malignant cells from focus T1 and T2 in patient P01 (left); bar chart summarizing functional enrichment of upregulated and downregulated genes (middle). Development trajectory of hepatocytes (right) in P01 inferred by monocle2, with cells colored by cell state (top) and sample origin (bottom). **(c)** Tumor focus size was negatively correlated with patient survival in both the HRA001748 and OEP000321 datasets. **(d)** Venn diagram illustrating the overlap of differentially expressed genes (left) and corresponding functional enrichment analysis (right). **(e)** Violin plots of the upregulated and downregulated overlap genes. **(f)** Chromatin accessibility peaks of *MCL1* in small and large tumor foci based on scATAC-seq data. **(g)** Expression distribution of *MCL1* across micro-lesions (MS), small lesions (S), and large lesions (L) in the public scRNA-seq dataset. **(h)** The spatial expression pattern of *MCL1* in P01_T1 (large lession) and P01_T2 (small lesion) samples was examined using Stereo-seq.]

We next asked whether these divergent evolutionary trajectories were accompanied by conserved malignant programmes. CNV-based profiling resolved six hepatocyte clusters, with diploid C5 representing normal hepatocytes (Hep_N) and CNV-altered C1–C4 and C6 representing malignant hepatocytes (Hep_M), supported by matched scATAC-seq profiles (**Fig. 3a, Supplementary Fig. 6a,b**). Hep_M subclusters showed marked patient- and lesion-specific segregation, with substantial variation in malignant cell abundance across tumor foci (**Fig. 3b**). Despite this heterogeneity, Hep_M populations shared aggressive cellular states, with enhanced differentiation potential in P01, P02 and P05 and concordant transcriptional and chromatin-accessibility programmes across subclusters (**Fig. 3c,d**). Functional analyses

revealed lesion-specific adaptations, including alcohol-associated responses, altered Golgi trafficking and metabolism, and viral-response programmes (**Fig. 3d, right**).



[**Fig. 3 Inter-focal heterogeneity and shared oncogenic programs in malignant hepatocytes of multifocal HCC. (a)** Heatmap illustrating large-

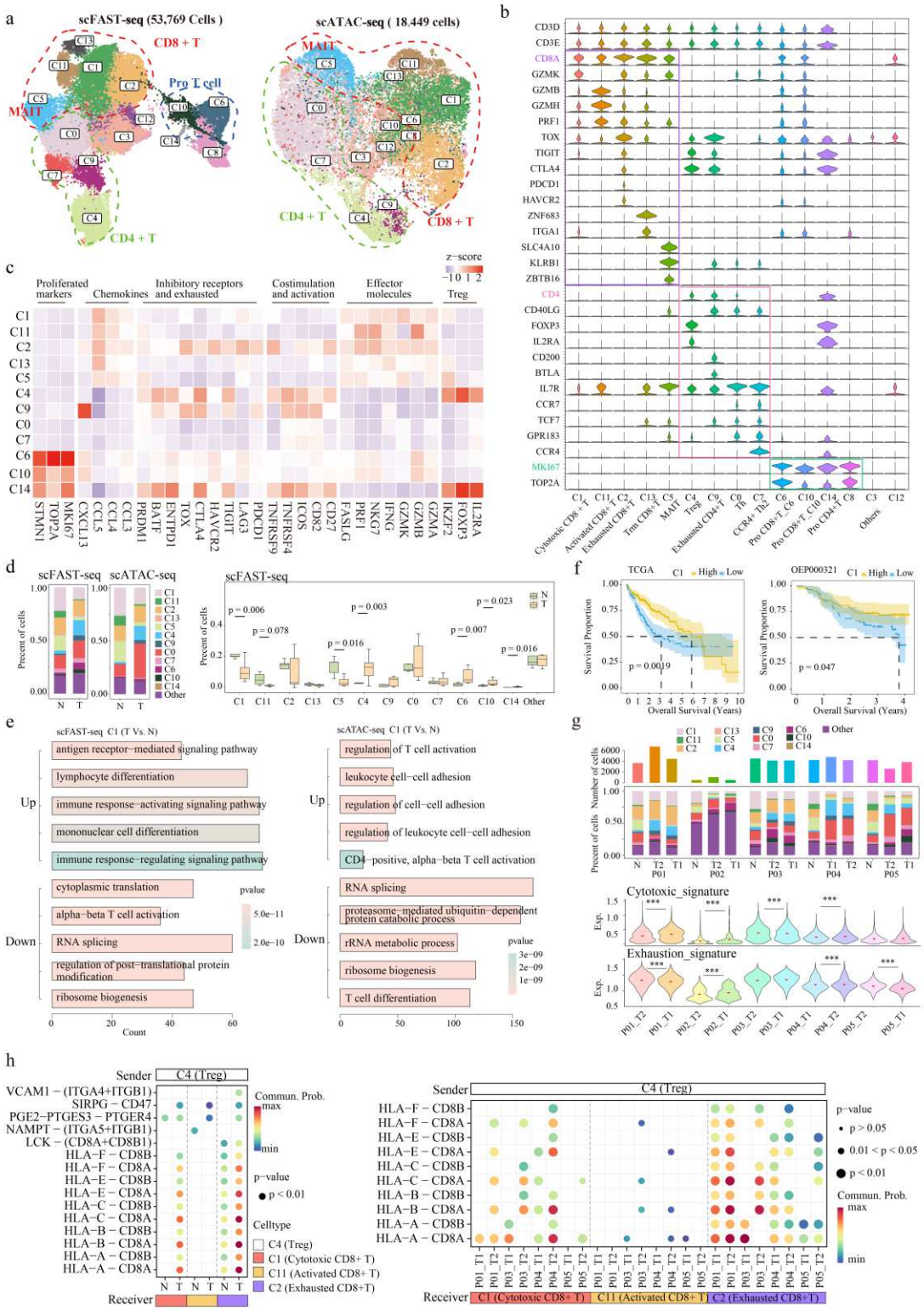
scale CNVs across individual hepatocytes (rows), with red indicating amplifications and blue indicating deletions. Cluster C5 corresponds to normal hepatocytes (Hep_N), while clusters C1-C4, and C6 represent malignant hepatocytes (Hep_M). **(b)** Stacked bar charts showing the distribution of samples within each cluster in scRNA-seq (left) and scATAC-seq (right). Stacked bar charts showing the proportions of Hep_M and Hep_N cells (bottom). **(c)** Boxplots depicting the differentiation potential of hepatocytes across different samples. **(d)** Heatmaps displaying differentially expressed genes and differentially accessible chromatin peaks across hepatocyte clusters (left). Venn diagram showing the overlap between genes in scFAST-seq and scATAC-seq (peak corresponding genes) (middle), alongside functional enrichment analysis of overlapping genes (right). **(e)** Venn diagram representing the intersection of upregulated genes among Hep_M clusters, with corresponding enrichment analysis of shared genes. **(f)** Violin plots showing the expression levels of *GPC3*, *EIF3E*, *EMC2*, *TMED2*, and *MTX2* in scFAST-seq and the public scRNA-seq dataset. **(g)** Spatial expression patterns of *TMED2* (left). Kaplan-Meier survival curves of *TMED2* (right). **(h)** Transwell assays were performed to determine the effect of *TMED2* overexpression or knockdown on the migration of HepG2 cells. CCK-8 assays were performed to examine the effect of *TMED2* overexpression or knockdown on the proliferative ability of HepG2 cells.]

Further analysis revealed a conserved malignant programme in Hep_M cells, characterised by increased biosynthetic and metabolic activity and reduced cell-adhesion and immune-related pathways compared with Hep_N cells (**Fig. 3e, Supplementary Fig. 6c,d**), consistent with findings from public HCC scRNA datasets (**Supplementary Fig. 7**). Cross-dataset integration identified four consistently upregulated genes, including *TMED2*, *EIF3E*, *EMC2* and *MTX2*, and 18 downregulated genes, including *TAT*, *SLC22A1* and *CYP2A6* (**Fig. 3f, Supplementary Fig. 8a**). Spatial transcriptomics confirmed

recurrent yet heterogeneous expression across tumor foci, while *TMED2*, *EIF3E* and *MTX2* were associated with poorer survival (**Fig. 3g, Supplementary Fig. 8b–f**). Functional perturbation showed that depletion of *TMED2* or *EMC2* impaired HCC cell proliferation and migration, whereas *TMED2* overexpression enhanced malignant phenotypes **(Fig. 3h, Supplementary Fig. 8g–i),** consistent with their reported oncogenic roles in other cancers[18-21]. Collectively, multifocal HCC exhibits divergent clonal evolution and substantial malignant heterogeneity, yet retains conserved oncogenic programmes, exemplified by *TMED2*.

Immunosuppressive T-cell remodeling underlying CD8+ T-cell dysfunction in multifocal HCC

Despite malignant heterogeneity and evolutionary divergence across tumor foci, we next investigated the T-cell ecosystem in multifocal HCC. Integration of matched scFAST-seq and scATAC-seq datasets identified 15 transcriptionally distinct T-cell clusters, which were further annotated into 12 canonical T-cell subsets, including cytotoxic CD8+ T (C1), activated CD8+ T (C11), exhausted CD8+ T (C2), tissue-resident memory CD8+ T (Trm CD8+ T, C13), mucosal-associated invariant T (MAIT, C5), proliferative CD8+ T (Pro CD8+, C6 and C10), regulatory T cells (Tregs, C4), exhausted CD4+ T (C9), helper T (Th, C0), CCR4+ Th2 (C7), and proliferative CD4+ T (Pro CD4+, C14) **(Fig. 4a–c**). Three minor clusters (C3, C8, C12) lacking definitive lineage markers were designated as "Others". Cell identity was consistently supported by functional enrichment analyses and label transfer from matched scATAC-seq datasets (**Supplementary Fig. 9a,b**).



[**Fig. 4 T-cell composition, functional states, and intercellular communication landscapes in multifocal HCC. (a)** UMAP plots showing T cell lineages identified in scFAST-seq (left) and scATAC-seq (right). **(b)** Violin plots displaying the expression of subtype-specific marker genes across T cell

subtypes, including cytotoxic CD8+ T cells (C1), activated CD8+ T cells (C11), exhausted CD8+ T cells (C2), tissue-resident memory CD8+ T cells (Trm CD8+ T, C13), mucosal-associated invariant T cells (MAIT, C5), proliferative CD8+ T cells (Pro CD8+ T, C6 and C10), regulatory T cells (Tregs, C4), exhausted CD4+ T cells (C9), helper T cells (Th, C0), CCR4+ Th2 cells (C7), and proliferative CD4+ T cells (Pro CD4+ T, C14). Three minor clusters lacking definitive lineage markers (C3, C8 and C12) were designated as "Others". **(c)** Heatmap of scaled normalized gene expression across T cell clusters. **(d)** Stacked bar charts showing the proportion of T cell subtype contained in adjacent non-tumor and tumor samples from scFAST-seq (left) and scATAC-seq (middle). Boxplots showing the variation in T cell subtype proportions between adjacent non-tumor and tumor samples (right). **(e)** Functional enrichment of cytotoxic CD8+ T (C1) cell DEGs in tumor tissues identified by scFAST-seq (left) and scATAC-seq (right). **(f)** Kaplan–Meier survival analysis of Cytotoxic CD8+ T cells (C1) in TCGA-LIHC and OEP000321 datasets. **(g)** Stacked bar charts showing T cell subtype composition across different patient samples (upper). Cytotoxic and exhaustion-related signature scores across tumor foci, compared using t-tests (bottom). **(h)** Receptor-ligand pairs showing significant differences between adjacent non-tumor and tumor tissues (left), and across tumor foci (right)**,** based on Treg (C4) and CD8+ T cell clusters. Dot size represents the p-value, and color reflects communication probability.]

Next, we compared the distribution of T cell subtypes between tumor and adjacent non-tumor tissues (**Fig. 4d)**, and identified differentially expressed genes (**Supplementary Fig. 9c)**. Notably, cytotoxic CD8+ T cells (C1), activated cytotoxic CD8+ T cells (C11), and MAIT cells (C5) were significantly decreased in tumor tissues (**Fig. 4d**), reflecting impaired cytotoxic T lymphocyte (CTL) infiltration. Interestingly, despite their reduced presence, cytotoxic CD8+ T cells in tumors retained transcriptional activity in immune-

related pathways such as lymphocyte differentiation, antigen receptor-mediated signaling, and immune response activation (**Fig. 4e**), suggesting partial preservation of effector potential. Similarly, residual MAIT cells exhibited immune activation signatures, suggesting that they may retain functional potential (**Supplementary Fig. 9d)**. Importantly, higher expression of the C1- and C5-associated gene signatures was significantly associated with better patient survival (**Fig. 4f, Supplementary Fig. 9e**), underscoring their potential role in orchestrating effective antitumor responses.

In contrast, immunosuppressive and dysfunctional T-cell populations were preferentially expanded in tumor tissues. Tregs (C4) were markedly enriched in tumor lesions, consistent with their role in suppressing antitumor immune responses (**Fig. 4d**). Proliferative CD8+ T cells (C6 and C10) and proliferative CD4+ T cells (C14) were also increased, potentially reflecting chronic antigen stimulation and dysfunctional immune activation (**Fig. 4d**). These alterations were consistently observed at both transcriptional and chromatin accessibility levels in matched scATAC-seq datasets (**Fig. 4e, Supplementary Fig. 9f-h**) and were further validated in independent single-cell datasets and bulk RNA-seq deconvolution analyses (**Supplementary Fig. 10 and 11**). Together, these findings demonstrate a broad remodeling of the T-cell compartment characterized by loss of cytotoxic immune populations and expansion of immunosuppressive or dysfunctional T-cell states in multifocal HCC.

Although the composition and magnitude of T-cell alterations varied among patients and tumor foci (**Fig. 4g, Supplementary Fig. 9h**), a common immunosuppressive pattern was observed across lesions. For example, P02 exhibited an immune-desert phenotype characterized by near-complete depletion of cytotoxic CD8+ T cells (C1), whereas P01 displayed intra-lesional differences in T-cell states, with the larger lesion (T1) retaining stronger cytotoxic activity and the smaller lesion (T2) showing increased exhaustion signatures. P05 exhibited uniformly reduced T-cell infiltration and limited

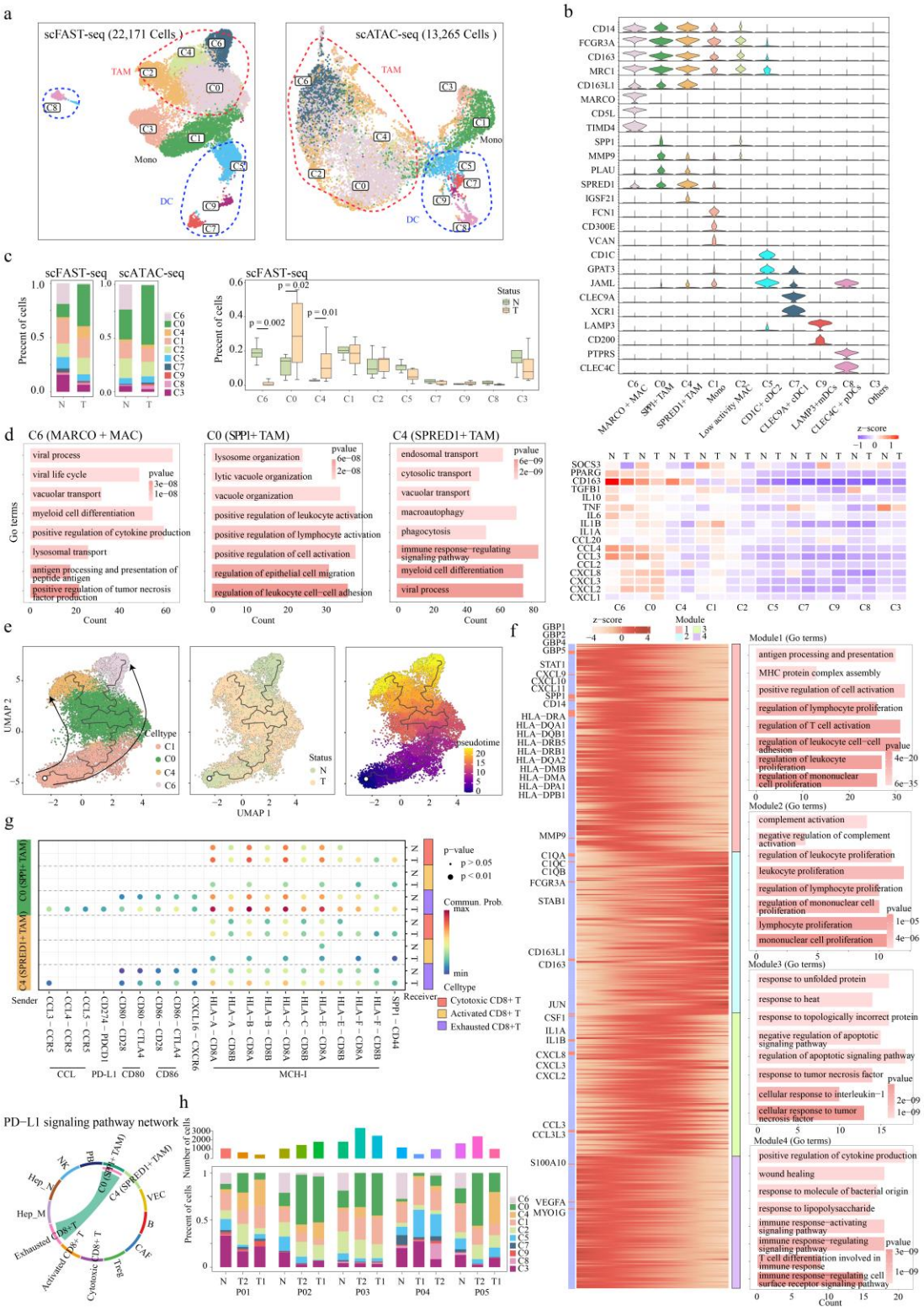
cytotoxic activity across tumor foci, consistent with advanced multifocal disease (~8 cm, stage C). These observations indicate that, despite variable immune compositions, multifocal HCC consistently develops an impaired cytotoxic immune environment.

To investigate potential mechanisms underlying T-cell dysfunction, we next analyzed intercellular communication among T-cell subsets (**Fig. 4h**). Tregs (C4) consistently emerged as the dominant immunosuppressive population across tumor lesions and exhibited extensive interactions with CD8+ T-cell subsets. Among these, both exhausted and cytotoxic CD8+ T cells received the strongest Treg-derived suppressive signals, whereas activated CD8+ T cells were comparatively less affected, suggesting a hierarchical program of T-cell suppression (**Fig. 4h**). Although MHC-I molecules (HLA-A/B/C) are classically recognized as mediators of antigen presentation to CD8+ T cells[22], our findings suggest that tumor-associated Tregs may exploit MHC-I-related interactions to modulate CD8+ T-cell states within the immunosuppressive tumor microenvironment.

Importantly, although the strength of Treg-mediated MHC-I interactions varied among tumor foci, this interaction pattern was consistently observed across multifocal lesions (**Fig. 4h**). For instance, stronger MHC-I interactions in P01_T2 were accompanied by increased CD8+ T-cell exhaustion compared with P01_T1, whereas uniformly weak signaling in P05 was consistent with its immune-desert phenotype. Collectively, these findings identify a conserved Treg-mediated MHC-I–CD8 interaction module associated with impaired cytotoxic immunity in multifocal HCC, suggesting a potential mechanism by which Tregs contribute to CD8+ T-cell dysfunction across diverse tumor foci.

SPP1+/SPRED1+ TAMs mediate conserved immunosuppressive interactions with exhausted CD8+ T cells through PD-L1 and CD80/CD86 signaling in multifocal HCC

Beyond T-cell-mediated suppression, we next explored whether myeloid populations represent additional conserved immunosuppressive components across divergent tumor foci. We therefore characterized the myeloid compartment using scFAST-seq. Unsupervised clustering identified 22,171 myeloid cells comprising ten transcriptionally distinct populations (**Fig. 5a**). Three major macrophage populations were defined, including tissue-resident MARCO+ macrophages (MARCO+ MACs, C6), SPP1+ tumor-associated macrophages (SPP1+ TAMs, C0), and SPRED1+ tumor-associated macrophages (SPRED1+ TAMs, C4), together with monocytes and multiple dendritic-cell subsets, including undifferentiated monocytes (Mono, C1), inactive/exhausted macrophages (C2), conventional dendritic cells (CD1C+ cDC2, C5; CLEC9A+ cDC1, C7), mature DCs (LAMP3+ mDCs, C9), plasmacytoid DCs (CLEC4C+ pDCs, C8), and a low-quality cluster (C3) (**Fig. 5b**). Cell identities were independently confirmed by matched scATAC-seq profiles (**Fig. 5a, Supplementary Fig. 12a**).



[**Fig. 5 Characterization of myeloid cell states and immunosuppressive interactions across multifocal HCC. (a)** UMAP plots showing the distribution of Mye cell lineages identified in scFAST-seq (left) and scATAC-seq (right). **(b)** Violin plots showing the expression of marker genes across

myeloid (Mye) subtypes, including tissue-resident MARCO+ macrophages (MARCO+ MACs, C6), SPP1+ tumor-associated macrophages (SPP1+ TAMs, C0), SPRED1+ tumor-associated macrophages (SPRED1+ TAMs, C4), monocytes (Mono, C1), conventional dendritic cells (CD1C+ cDC2, C5; CLEC9A+ cDC1, C7), mature dendritic cells (LAMP3+ mDCs, C9), plasmacytoid dendritic cells (CLEC4C+ pDCs, C8), inactive/exhausted macrophages (C2), and a low-quality cluster (C3). **(c)** Stacked bar charts showing the proportions of Mye subtypes in adjacent non-tumor and tumor samples from scFAST-seq (left) and scATAC-seq (middle). Boxplots comparing the abundance of Mye subtypes between non-tumor and tumor tissues (right). **(d)** Functional enrichment analysis (left) for clusters MARCO+ MACs (C6), SPP1+ TAMs (C0), and SPRED1+ TAMs (C4). Heatmap displaying scaled normalized expression of chemokines, inflammatory genes, and immunosuppressive factors across different Mye subtypes (right). **(e)** Development trajectory of MARCO+ MACs (C6), SPP1+ TAMs (C0), SPRED1+ TAMs (C4), and undifferentiated monocytes (C1) inferred by monocle3. **(f)** Heatmap showing pseudotime-ordered differentially expressed genes, annotated with representative genes and associated GO terms for each trajectory branch. **(g)** Receptor–ligand interaction analysis between SPP1+ TAMs (C0)/SPRED1+ TAMs (C4) and CD8+ T cells, highlighting key signaling differences between tumor and adjacent non-tumor tissues (upper). The inferred PD-L1 signaling network (bottom). **(h)** Stacked bar charts illustrating the distribution of Mye subtypes across different tumor foci.]

Compared with adjacent tissues, tumor lesions exhibited profound remodeling of the macrophage compartment, characterized by depletion of MARCO+ MACs (C6) and marked expansion of both SPP1+ TAMs (C0) and SPRED1+ TAMs (C4) (**Fig. 5c, Supplementary Fig. 12b**). MARCO+ MACs (C6) retained transcriptional programs associated with antiviral responses and myeloid differentiation(**Figures 5d and S12c**), consistent with homeostatic

Kupffer-cell functions, acting as sentinels to maintain tissue homeostasis[23]. In contrast, SPP1+ TAMs (C0) displayed inflammatory and immunoregulatory features, including activation of lysosomal organization, leukocyte activation, and cell-adhesion pathways (**Fig. 5d, Supplementary Fig. 12c**). Notably, these cells highly expressed chemokines (e.g., CCL, CXCL chemokines), inflammatory mediators (IL-1α, IL-1β), and immunosuppressive factors (IL-10, TGF-β1). SPRED1+ TAMs (C4) preferentially activated endosomal trafficking and autophagy programs involved in viral immune responses, suggesting that they may regulate inflammatory activation through these pathways (**Fig. 5d, Supplementary Fig. 12c**). Similar macrophage remodeling was consistently observed in independent HCC scRNA-seq cohorts (**Supplementary Fig. 13**).

Trajectory reconstruction further demonstrated that tumor-associated macrophages arise through active reprogramming rather than selective expansion. In adjacent tissues, Mono (C1) differentiated predominantly toward homeostatic MARCO+ MACs (C6) through an intermediate SPP1+ state. In contrast, within tumors, Mono (C1) differentiation was redirected toward suppressive SPRED1+ TAMs through SPP1+ intermediates, indicating a tumor-driven macrophage fate switch **(Fig. 5e)**. Pseudotime-dependent gene module analysis further supported progressive acquisition of suppressive macrophage programs during differentiation **(Fig. 5f).**

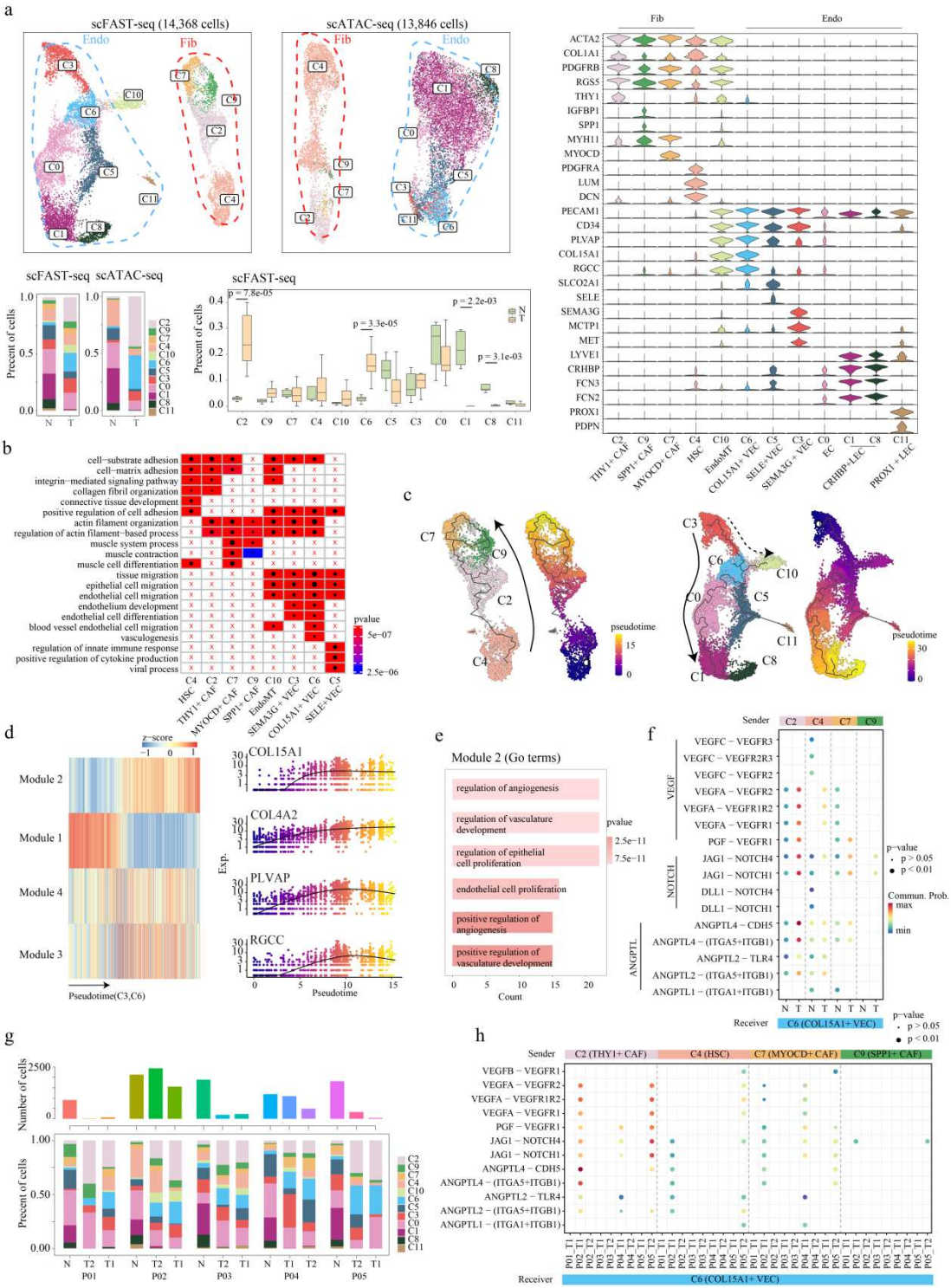
We next investigated whether macrophage heterogeneity converges on conserved immunosuppressive communication programs. Despite marked differences in macrophage composition across lesions, SPP1+ and SPRED1+ TAMs consistently emerged as the dominant suppressive populations. Cell-cell communication analysis revealed extensive interactions between SPP1+/SPRED1+ TAMs and CD8+ T cells mediated by PD-L1 (CD274), CD80/CD86, MHC-I, and CCL signaling pathways, with substantially stronger signaling in tumor than adjacent tissues across patients and tumor foci (**Fig. 5g, Supplementary Fig. 14a-c**). Exhausted CD8+ T cells represented the principal recipients of TAM-derived suppressive signals, followed by cytotoxic

CD8+ T cells (**Fig. 5g**), indicating preferential reinforcement of T-cell dysfunction during tumor evolution. Notably, SPP1+ TAMs exhibited particularly strong engagement of exhausted CD8+ T cells through the CD274–PDCD1 and CD80/CD86–CTLA4/CD28 axes (**Fig. 5g, Supplementary Fig. 14a,c**), highlighting these cells as major mediators of immune evasion and potential determinants of immunotherapy resistance. MHC-I-dependent interactions closely mirrored those observed in Tregs (**Fig. 4k,l**), suggesting that distinct suppressive cell populations converge on a common immunoregulatory program.

Although TAM abundance and signaling intensity varied considerably among individual lesions, the overall suppressive communication architecture remained highly conserved (**Fig. 5h, Supplementary Fig. 14b,c**). For example, P03 exhibited the highest myeloid infiltration (**Fig. 1g**), whereas SPP1+ TAMs predominated in P01_T2 and P05_T2 and SPRED1+ TAMs were preferentially enriched in the corresponding T1 lesions (**Fig. 5h**). These compositional differences were accompanied by quantitative variation in macrophage–T-cell signaling strength but did not alter the core suppressive network **(Supplementary Fig. 14c)**. Collectively, these findings demonstrate that SPP1+/SPRED1+ TAMs constitute a conserved immunosuppressive hub that transcends profound inter-focal heterogeneity, engaging cytotoxic and exhausted CD8+ T cells through PD-L1, CD80/CD86, and MHC-I signaling. Together with the Treg-mediated suppressive program identified above, these results establish that genetically and evolutionarily distinct tumor foci converge on a shared immunosuppressive microenvironments.

Convergent expansion of THY1+ CAFs and COL15A1+ VECs accompanies inter-focal heterogeneity in stromal remodeling and angiogenesis in multifocal HCC

Stromal cells, including fibroblasts and endothelial cells, are key regulators of immune modulation, extracellular matrix (ECM) remodeling, and angiogenesis in the HCC microenvironment[24]. Analysis of 14,368 fibroblast (Fib) and endothelial (Endo) cells identified 12 transcriptionally distinct clusters (**Fig. 6a, left**). Fibroblast populations consisted of THY1+ CAFs (C2), SPP1+ CAFs (C9), MYOCD+ CAFs (C7), and hepatic stellate cells (HSCs, C4). The endothelial cell compartment was composed of generic endothelial cells (ECs, C0), vascular endothelial cells (VECs) including COL15A1+ (C6), SELE+ (C5), and SEMA3G+ (C3) subsets, as well as lymphatic endothelial cells (LECs), including CRHBP+ (C1, C8) and PROX1+ (C11) populations. (**Fig. 6a, right**). Cluster C10 co-expressed fibroblast and endothelial markers, suggesting a transitional stromal population. Cell identities were independently confirmed by matched scATAC-seq data (**Fig. 6a, Supplementary Fig. 15a**).



[**Fig. 6 Fibroblast and endothelial cell states and stromal–vascular interactions across multifocal HCC. (a)** UMAP plots (left) displaying the distribution of fibroblast (Fib) and endothelial (Endo) cell lineages in scFAST-seq and scATAC-seq. Violin plots (right) showing the expression of representative marker genes across Fib and Endo subtypes, including THY1+ cancer-associated fibroblasts (CAFs; C2), SPP1+ CAFs (C9), MYOCD+ CAFs

(C7), and hepatic stellate cells (HSCs; C4), as well as COL15A1+ (C6), SELE+ (C5), and SEMA3G+ (C3) vascular endothelial cells (VECs), and CRHBP+ (C1/C8) and PROX1+ (C11) lymphatic endothelial cells (LECs). Cluster C10 co-expressed fibroblast and endothelial markers, suggesting a transitional stromal population. Stacked bar charts illustrating the proportions of Fib and Endo subtypes in adjacent non-tumor and tumor tissues, based on scFAST-seq (left) and scATAC-seq (right). Boxplots comparing the abundance of Fib and Endo subtypes between adjacent non-tumor and tumor samples. **(b)** Functional enrichment analysis of identified cell clusters. “x” indicates no significant enrichment, and dot size reflects gene count. **(c)** Developmental trajectories of Fib (left) and Endo (right) cells inferred by Monocle3. **(d)** Heatmap showing differentially expressed genes modules arranged in pseudo temporal patterns (left). The expression dynamics of *COL15A1*, *COL4A2*, *PLVAP*, and *RGCC* in module 2 are highlighted. **(e)** Functional enrichment of genes in module 2. **(f)** Receptor–ligand interaction analysis between Fib subtypes and COL15A1+ VEC (C6), highlighting key signaling differences between tumor and adjacent non-tumor tissues. **(g)** Bar plots showing the distribution of fibroblast and endothelial subtypes across patients and lesions. **(h)** Receptor–ligand interaction analysis between Fib subtypes and COL15A1+ VEC (C6), highlighting key signaling differences between lesions.]

Compared with adjacent tissues, tumors consistently exhibited expansion of THY1+ cancer-associated fibroblasts (CAFs) (C2) and COL15A1+ vascular endothelial cells (VECs) (C6), accompanied by depletion of CRHBP+ lymphatic endothelial cells (LECs) (C1, C8) (**Fig. 6a, Supplementary Fig. 15b–g**). THY1+ CAFs (C2) preferentially activated cell–matrix adhesion, actin cytoskeleton organization, and vesicle transport programs, consistent with active ECM remodeling (**Fig. 6b, Supplementary Fig. 16a**). In parallel, COL15A1+ VECs (C6) displayed differentiation and

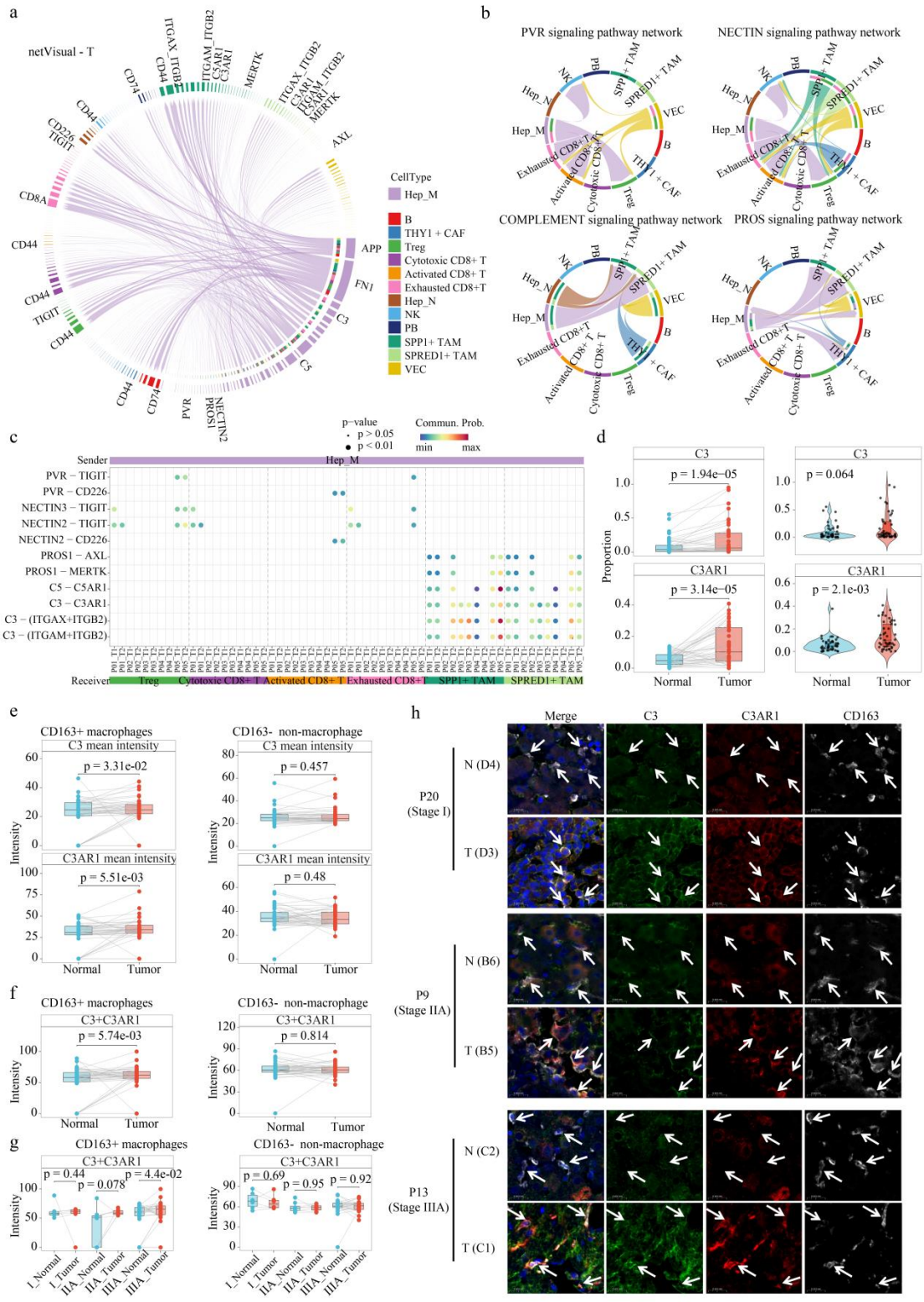
angiogenic signatures characteristic of immature endothelial cells (**Fig. 6b, Supplementary Fig. 16b**), whereas loss of CRHBP+ LECs (C1 and C8) suggested impaired lymphatic function and immune cell trafficking (**Supplementary Fig. 16c**). These findings indicate a conserved stromal shift toward matrix remodeling and angiogenesis across multifocal HCC.

Trajectory analysis further revealed coordinated stromal reprogramming during tumor progression. Fibroblasts differentiated from HSCs through THY1+ CAFs (C2) before diverging into SPP1+ CAFs (C9) and MYOCD+ CAFs (C7), consistent with progressive ECM deposition and stromal activation **(Fig. 6c)**. Endothelial cells followed a developmental trajectory from SEMA3G+ VECs (C3) to immature COL15A1+ VECs (C6) and subsequently to mature SELE+ VECs (C5) , with a pseudotime-associated gene module (including *COL15A1*, *COL4A2*, *PLVAP*, and *RGCC*) supporting vascular remodeling and angiogenesis **(Fig. 6d,e)**.

Cell–cell communication analysis demonstrated that THY1+ CAFs (C2) preferentially interacted with COL15A1+ VECs (C6) through ANGPTL, NOTCH, and VEGF signaling pathways, indicating coordinated regulation of stromal remodeling and neovascularization (**Fig. 6f**). Although CAF and VEC composition, together with signaling intensity, varied substantially among patients and tumor foci, the expansion of THY1+ CAFs (C2) and COL15A1+ VECs (6) was consistently observed across lesions (**Fig. 6g,h, Supplementary Fig. 16d**). These findings reveal coordinated stromal remodeling across multifocal HCC, characterised by recurrent expansion of THY1+ CAFs and COL15A1+ VECs and their coordinated activation of ECM remodelling and angiogenic programmes despite inter-focal heterogeneity.

Malignant hepatocytes exhibit conserved C3/C5 complement signaling with SPP1+/SPRED1+ TAMs across tumor foci in multifocal HCC

During multifocal HCC progression, effector immune and stromal populations progressively declined, whereas immunosuppressive and tumor-promoting cell populations expanded (**Supplementary Fig. 17a**). These trends were consistently reproduced in scATAC-seq and independent public scRNA-seq datasets despite marked inter- and intra-patient heterogeneity (**Supplementary Fig. 17a,b**). For example, P01 retained relatively T cell-rich lesions, whereas P02 was dominated by malignant hepatocytes and stromal cells, illustrating the diverse immune landscapes across multifocal lesions.



[**Fig. 7 Malignant hepatocyte-centered signaling networks and macrophage-specific complement activation in multifocal HCC. (a)** Chord diagram showing ligand–receptor interactions through which Hep_M cells communicate with other cell populations in tumor tissues. **(b)** Chord diagrams

illustrating interactions between Hep_M cells and CD8+ T cells or TAMs mediated by PVR and NECTIN2 (upper), and C3/C5 COMPLEMENT and PROS (bottom) signaling pathways. **(c)** Bubble plot showing interaction strength of ligand–receptor pairs associated with PVR, NECTIN2, COMPLEMENT, and PROS signaling across tumor foci. **(d)** Quantification of C3- and C3AR1-positive cells in tumor and adjacent tissues. **(e)** Expression intensity of C3 and C3AR1 in CD163+ macrophages and CD163−non-macrophage populations. **(f)** Quantification of C3−C3AR1 signaling intensity in macrophage and non-macrophage compartments. **(g)** Stage-stratified analysis of C3–C3AR1 activation in CD163+ macrophages and CD163− populations. **(h)** Representative mIHC images showing C3 and C3AR1 expression in CD163+ macrophages across representative multifocal HCC cases. N: Adjacent normal, T: tumor, Scale bars, 20 um.]

Having established heterogeneous cellular states accompanied by recurrent remodeling patterns across malignant, immune, and stromal compartments, we next investigated how these distinct populations communicate to shape conserved immunosuppressive ecosystems. We systematically mapped intercellular communication networks across tumor foci. Among all cell populations, Hep_M emerged as a dominant signaling hub, exhibiting extensive interactions with CD8+ T cells, SPP1+/SPRED1+ TAMs, and CAFs (**Supplementary Fig. 18a,b**). A tumor-enriched, non-classical PVR/NECTIN2 immune checkpoint axis was activated in Hep_M cells, engaging TIGIT on exhausted CD8+ T cells and Tregs and CD226 on activated CD8+ T cells. This signaling program displayed marked inter-patient variation, with enhanced activation primarily observed in tumor foci from P01 and P05 (**Fig. 7a,b, Supplementary Fig. 19a–c**).

In contrast, Hep_M consistently engaged SPP1+/SPRED1+ TAMs through COMPLEMENT signaling (C3–C3AR1/ITGAX–ITGB2/ITGAM–ITGB2 and C5–C5AR1) and PROS signaling (PROS1–AXL/MERTK) across most

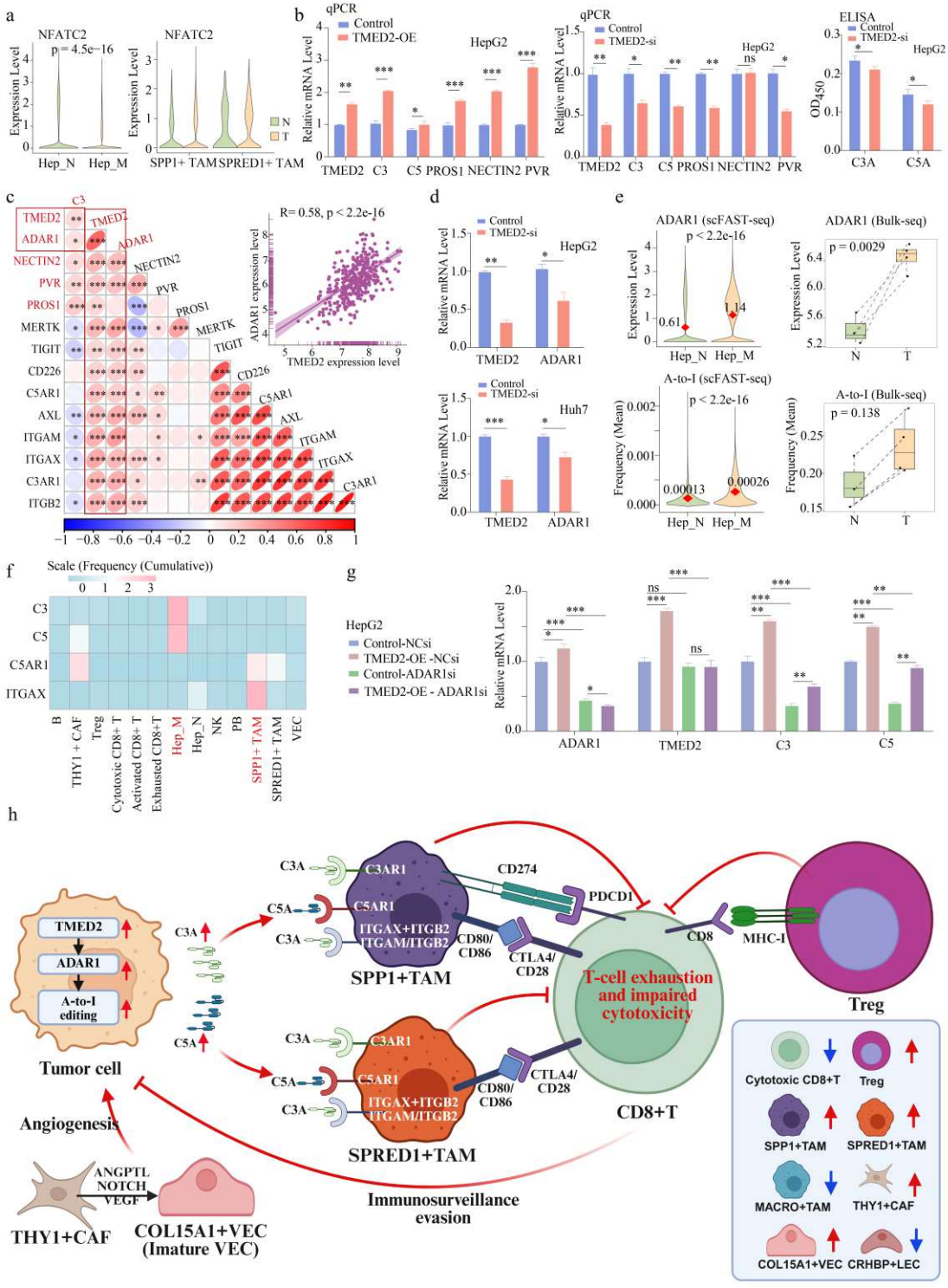
patients and tumor foci, whereas these interactions were absent in Hep_N (**Fig. 7b,c, Supplementary Fig. 19a,c,d**). This finding extends previous evidence implicating C3/C5 complement signaling in M2-like macrophage polarization and suppression of antitumor T cell responses[25, 26], and further reveals a tumor cell–derived complement mechanism whereby malignant hepatocytes drive SPP1+/SPRED1+ TAM reprogramming and establish a conserved immunosuppressive microenvironments across heterogeneous tumor foci. These interactions were independently validated by scATAC-seq, public scRNA-seq datasets, and spatial transcriptomics (**Supplementary Fig. 20a–d, Supplementary Fig. 21a–c**), demonstrating that, despite profound inter-focal heterogeneity, malignant hepatocytes converge on a shared complement-dependent program to remodel macrophage function and promote immune suppression.

To validate the Hep_M–TAM complement axis identified by single-cell and spatial analyses, we performed mIHC on a tissue microarray containing 48 paired multifocal HCC tumors and matched adjacent tissues (**Supplementary Fig. 22a**). Compared with adjacent normal tissues, tumor tissues showed a significantly higher proportion of C3AR1+ cells **(Fig. 7d)**. The proportion of C3+ cells was also increased in tumor tissues, with the difference reaching statistical significance in paired patient-matched analysis, whereas the unpaired comparison showed only a borderline trend (P = 0.064) **(Fig. 7d)**. In contrast, CD163+ macrophages were markedly reduced in tumor tissues (**Supplementary Fig. 22b**). Importantly, elevated C3 and C3AR1 expression intensity was selectively observed within CD163+ macrophages in tumor tissues (**Fig. 7e,f)**, while CD163- non-macrophage populations showed no significant differences between tumor and adjacent tissues (**Fig. 7e,f**). Moreover, tumor-specific activation of C3–C3AR1 signaling in CD163+ macrophages showed a trend toward enhanced activation with advanced clinical stages of multifocal HCC but was absent in adjacent tissues (**Fig. 7g,h, Supplementary Fig. 22c,d**). This activation pattern was not associated with

patient age or sex (**Supplementary Fig. 22e,f**). Statistical significance was observed in Stage IIIA tumors (P = 0.044), whereas Stage I (P = 0.44) and Stage IIA (P = 0.078) tumors showed similar trends without reaching statistical significance (**Fig. 7g)**, potentially reflecting the limited sample size and inter-patient heterogeneity. Together, these findings establish a conserved Hep_M–SPP1+/SPRED1+ TAM C3/C5 complement axis across heterogeneous tumor foci, identifying malignant hepatocytes as key regulators of macrophage reprogramming and convergent immunosuppression in multifocal HCC.

A TMED2–ADAR1 RNA editing axis regulates tumor-intrinsic C3/C5 complement signaling in multifocal HCC

Previous studies have implicated a *NFAT1* (*NFATC2*)-dependent C3a/C3aR–Ca^{2+} feedback loop in TAM polarization[25]. However, *NFATC2* was downregulated in Hep_M cells and showed no differential expression in TAMs between tumor and adjacent tissues (**Fig. 8a**), suggesting that the activated Hep_M–TAM C3/C3AR1 axis in multifocal HCC is driven by NFATC2-independent mechanisms.



[**Fig. 8 TMED2–ADAR1-mediated RNA editing shapes C3/C5 complement signaling axis linked to immunosuppressive TAMs in multifocal HCC. (a)** Expression of *NFATC2* in malignant hepatocytes (Hep_M) and normal hepatocytes (Hep_N) (left), and in TAM subsets (right) from multifocal HCC. **(b)** qPCR detecting the Hep_M–TAM communication molecules after *TMED2* knockdown (left) or overexpression (midle) in HepG2 cells. Secreted

C3A/C5A following *TMED2* knockdown (right). **(c)** Correlation analysis of *TMED2* expression with *ADAR1* and Hep_M–TAM communication molecules in the TCGA-LIHC cohort. **(d)** *ADAR1* mRNA changes after *TMED2* knockdown in HepG2/Huh7 cells. **(e)** *ADAR1* expression and global A-to-I editing in Hep_M vs. Hep_N cells (left) and multifocal HCC vs. normal tissues (right). **(f)** Heatmap of A-to-I editing frequencies across cell types. **(g)** Rescue experiments demonstrating that *ADAR1* depletion attenuates TMED2-induced activation of C3/C5 expression. **(h)** Proposed model illustrating the TMED2–ADAR1–complement axis in malignant hepatocytes and its role in TAM reprogramming and immune suppression in multifocal HCC.]

Given that *TMED2* represents a shared malignant programme in multifocal HCC (**Fig. 3f–h**), we investigated whether it mediates tumor–immune communication. A pan-cancer analysis recently linked *TMED2* to immune features and prognosis[27], although its immunoregulatory mechanisms remain unclear. *TMED2* overexpression in HepG2 cells significantly increased the expression of immune-associated mediators, including *C3, C5, PROS1, PVR, and NECTIN2.* Following *TMED2* knockdown, the expression of *C3, C5, PROS1, and PVR* was reversed, whereas *NECTIN2* levels were not significantly altered (**Fig. 8b**). Consistently, depletion of *TMED2* markedly decreased C3a and C5a secretion (**Fig. 8b, right**), identifying *TMED2* as a tumor-intrinsic regulator of complement activation and broader tumor–immune communication programmes.

Given the emerging role of A-to-I RNA editing in shaping HCC immunity[28], we next examined whether *TMED2* regulates ADAR1-mediated RNA editing. *TMED2* expression positively correlated with *ADAR1* levels in TCGA-LIHC (**Fig. 8c**), and *TMED2* knockdown reduced *ADAR1* expression (**Fig. 8d**). Both Hep_M cells and tumor tissues showed increased *ADAR1* expression and a tendency toward elevated global A-to-I RNA editing levels, although the difference in bulk-seq samples did not reach statistical

significance (p = 0.138), potentially due to the limited sample size; meanwhile, preferential editing events were identified in *C3* and *C5* transcripts, whereas *C5AR1* and *ITGAX* editing occurred predominantly in TAMs (**Fig. 8e,f, Supplementary Fig. 23a–e)**. In contrast, no significant RNA editing was detected in *PROS1*, *NECTIN2*, or *PVR*. Importantly, *ADAR1* depletion attenuated, but did not completely eliminate, *TMED2*-induced *C3/C5* upregulation, suggesting that *TMED2* regulates complement activation through an *ADAR1*-associated mechanism with additional *ADAR1*-independent components (**Fig. 8g**).

Collectively, these findings define a Hep_M-centered immunoregulatory circuit in multifocal HCC, in which *TMED2* activates ADAR1-mediated A-to-I RNA editing to enhance C3/C5 complement signaling, thereby reprogramming TAMs toward an immunosuppressive state and establishing a conserved immune microenvironments across heterogeneous tumor foci (**Fig. 8h**). The TMED2–ADAR1 axis therefore represents a potential therapeutic vulnerability for disrupting immune evasion in multifocal HCC.

Discussion

Multifocal HCC provides a unique opportunity to investigate how divergent malignant evolution shapes multicellular tumor ecosystems. Previous studies have demonstrated substantial molecular differences among spatially separated tumor foci, indicating that distinct evolutionary histories generate heterogeneous malignant states[8, 12]. However, whether such malignant divergence is accompanied by equally divergent tumour ecosystems remains unclear. By integrating single-cell and spatial multi-omics with mIHC and functional validation, we demonstrate that extensive inter-focal heterogeneity coexists with shared oncogenic programmes and a conserved immunosuppressive ecosystem. Although tumour foci acquired distinct genomic, transcriptional, epigenetic, and evolutionary states, they recurrently retained shared malignant programmes, exemplified by *TMED2*, and

established similar immune, myeloid, stromal, and vascular states. These findings indicate that malignant evolution and tumour ecosystem organisation are not strictly coupled, suggesting that conserved ecological pressures may impose shared functional dependencies despite tumour-cell diversification.

Cancer evolution has traditionally been viewed as a process driven by genetic diversification, clonal selection, and acquisition of advantageous malignant traits[8, 13, 29]. Under this framework, molecularly distinct tumour populations would be expected to generate corresponding phenotypic and ecological differences. Our findings instead reveal that divergent malignant states can retain shared oncogenic programmes while independently establishing conserved tumour-supportive ecosystems. Spatially separated lesions displayed differences in chromatin accessibility, metabolic states, differentiation trajectories, and clonal evolution, yet repeatedly converged on immune suppression and microenvironmental remodelling. Thus, tumour evolution appears to involve both diversification and conservation, with heterogeneous malignant states retaining selected programmes that facilitate adaptation to a shared ecological context.

A defining feature of this conserved ecosystem was the recurrent establishment of immunosuppressive immune states across evolutionarily distinct tumour foci. Despite variation in T-cell composition among patients and lesions, tumour foci consistently exhibited Treg enrichment, reduced CD8+ T-cell infiltration and cytotoxicity, and recurrent interactions among Tregs, TAMs, and CD8+ T cells. SPP1+/SPRED1+ TAMs and Tregs formed complementary suppressive networks involving CD274–PDCD1, CD80/CD86–CTLA4/CD28, and MHC-I–CD8 interactions. Notably, MHC-I-associated interactions may extend beyond antigen presentation to participate in broader Treg–CD8+ T-cell regulatory networks. These findings suggest that immune suppression represents a conserved functional state rather than a fixed cellular composition, enabling distinct tumour foci to achieve similar

impairment of antitumour immunity through shared communication programmes.

Conservation was also observed in the myeloid and stromal compartments. Although macrophage proportions varied among lesions, SPP1+ /SPRED1+ TAMs repeatedly emerged across evolutionarily distinct tumour foci and exhibited extensive communication with malignant hepatocytes and T cells. Their recurrent presence suggests that TAM states are shaped not only by cellular origin but also by tumour-derived ecological signals, enabling functional adaptation while maintaining immunosuppressive properties. Similarly, THY1+ CAFs and COL15A1+ VECs were consistently enriched across tumour foci, despite differences in their activating signals. In addition, Hep_M populations also communicated with VECs and CAFs through EPHA, TRAIL, and AGT signalling pathways, potentially contributing to angiogenesis, apoptosis regulation, and extracellular matrix remodelling (**Supplementary Fig. 24**). These findings indicate that distinct malignant states can engage diverse molecular routes while converging on conserved fibrovascular architectures that support tumour growth and immune suppression.

A central question arising from these observations is how evolutionarily distinct malignant populations establish similar tumour ecosystems. Our data identify malignant hepatocytes as active regulators of this process and reveal *TMED2* as a shared oncogenic programme linked to conserved tumour–macrophage communication. Integrated cell–cell communication analyses and functional experiments identified a tumour-intrinsic TMED2–ADAR1-dependent C3/C5 complement regulatory axis connecting malignant hepatocytes with SPP1+/SPRED1+ TAMs. The persistence of *TMED2*-induced *C3/C5* upregulation after *ADAR1* depletion suggests that, although *ADAR1* is an important mediator of *TMED2*-driven complement activation, additional *ADAR1*-independent pathways may also contribute to this regulatory axis. This mechanism provides a potential explanation for how

divergent tumour foci repeatedly establish similar macrophage-associated immunosuppressive niches and suggests that shared tumour-intrinsic programmes may act as ecological organisers across heterogeneous lesions.

Complement signalling has emerged as an important regulator of tumour immunity by shaping macrophage activation and inflammatory states[30, 31]. However, previous studies have mainly focused on macrophage-intrinsic or immune-cell-derived complement regulation[25, 26, 32, 33]. Our findings identify a tumour-originated complement regulatory mechanism in multifocal HCC, in which malignant hepatocytes acquire complement-producing capacity through a TMED2–ADAR1-dependent RNA editing programme. A-to-I RNA editing represents an epitranscriptomic layer linking shared malignant programmes to C3/C5 expression and secretion, thereby enabling tumour cells to directly influence macrophage states. These findings extend current understanding of complement regulation from an immune-cell-centred model toward a tumour-initiated intercellular communication mechanism and establish the TMED2–ADAR1–C3/C5 axis as a mechanistic link between malignant programmes and conserved tumour–macrophage interactions.

The identification of shared oncogenic programmes and conserved immunosuppressive ecosystems has important therapeutic implications. Current immunotherapies, including immune checkpoint blockade, remain limited by complex and heterogeneous immunosuppressive networks in HCC[34, 35]. Our findings suggest that targeting lesion-specific genetic alterations alone may not fully address the shared ecological dependencies sustaining multifocal disease. Instead, targeting conserved tumour–immune interactions may provide a complementary strategy across genetically distinct tumour foci. The recurrent activation of tumour-derived complement-associated macrophage remodelling raises the possibility that disrupting the TMED2–ADAR1–C3/C5 axis could interfere with cross-focal tumour–macrophage dependencies and enhance antitumour immunity.

Several limitations should be acknowledged. First, although integrated single-cell and spatial multi-omics, mIHC validation, and functional experiments support the involvement of the TMED2–ADAR1–C3/C5 axis in tumour–macrophage communication, its therapeutic relevance requires further validation *in vivo* using multifocal HCC models and patient-derived systems. Second, the upstream mechanism by which *TMED2* regulates *ADAR1* and the specific A-to-I RNA editing events through which ADAR1 controls *C3/C5* expression remain unclear. Given that *TMED2* is a Golgi–endoplasmic reticulum protein trafficking regulator[36], future studies integrating trafficking analyses, *ADAR1* regulatory profiling, and site-specific RNA editing approaches will be required to define the complete TMED2–ADAR1–C3/C5 axis. Third, larger longitudinal cohorts are required to determine how shared oncogenic programmes and conserved tumour ecosystems evolve during disease progression and therapeutic selection.

In summary, our study demonstrates that malignant heterogeneity does not necessarily translate into functional heterogeneity of the tumour ecosystem in multifocal HCC. Spatially separated tumour foci undergo extensive genomic, transcriptional, epigenetic, and evolutionary diversification while retaining shared oncogenic programmes and repeatedly establishing conserved immunosuppressive ecosystems. The TMED2–ADAR1–C3/C5 complement axis provides a mechanistic link between shared malignant programmes and conserved tumour–macrophage interactions, revealing how divergent tumour foci achieve functional convergence. These findings establish a multi-omic and spatial framework for distinguishing lesion-specific malignant states from shared functional dependencies and highlight the TMED2–ADAR1–C3/C5 axis as a potential cross-focal therapeutic vulnerability in multifocal HCC.

Author's contributions

W.L.Z. conceived and supervised the study. W.L.Z. and C.W. designed the study. C.W. analyzed the data. C.W., S.M., and K.S. prepared materials for

scFAST-seq, scATAC-seq, Stereo-seq, and bulk RNA-seq. K.S. performed the experiments for validation. C.W., Z.H.J., D.Y.L., and H.P.Z. designed and constructed the website. C.W., W.L.Z. interpreted data. S.M., N.N.S., and W.L.L curated the clinical data. C.W. and W.L.Z. wrote and revise the manuscript. All authors read and approved the manuscript.

Fundings

This study was supported by the National Natural Science Foundation of China (Grant No. 32400553 and 32100513), the Postdoctoral Fellowship Program of CPSF (Grant No. GZC20230617), the Guangdong-Hong Kong-Macau Joint Laboratory for Cell Fate Regulation and Diseases, China (Grant No. 2022LSYS008), the Shenzhen Clinical Research Center for Rare Diseases (Grant No. LCYSSQ20220823091402005), and the Sanming Project of Medicine in Shenzhen (Grant No. SZSM202311022).

Data availability

Raw scFAST-seq, scATAC-seq, single-cell spatial transcriptomic, and in-house bulk RNA-seq datasets have been deposited in the GSA database (accession numbers: HRA015013, HRA015779, HRA016973, and HRA017034, respectively). Processed scFAST-seq and scATAC-seq expression matrices are available via GEO (GSE322705 and GSE324115). Public scRNA-seq data HRA001748[16] were downloaded from the Genome Sequence Archive (https://ngdc.cncb.ac.cn/gsa-human/browse/HRA001748). the full dataset can be explored interactively at http://www.biomedical-web.com/hccOmics/. Analysis code is available at GitHub (https://github.com/Wucheng-tech/HCC). Public bulk RNA-seq datasets included TCGA-LIHC (UCSC Xena, https://xena.ucsc.edu/) and OEP000321 (HCCDB v2.0[17]).

Conflict of interest statement

All authors declare no competing financial interests.

References

1. Singal AG, Kanwal F, Llovet JM. Global trends in hepatocellular carcinoma epidemiology: implications for screening, prevention and therapy. Nat Rev Clin Oncol. 2023; 20(12):864-84.
2. Roayaie S, Jibara G, Tabrizian P, et al. The role of hepatic resection in the treatment of hepatocellular cancer. Hepatology. 2015; 62(2):440-51.
3. Fukami Y, Kaneoka Y, Maeda A, et al. Liver Resection for Multiple Hepatocellular Carcinomas: A Japanese Nationwide Survey. Ann Surg. 2020; 272(1):145-54.
4. Singal AG, Llovet JM, Yarchoan M, et al. AASLD Practice Guidance on prevention, diagnosis, and treatment of hepatocellular carcinoma. Hepatology. 2023; 78(6):1922-65.
5. Furuta M, Ueno M, Fujimoto A, et al. Whole genome sequencing discriminates hepatocellular carcinoma with intrahepatic metastasis from multi-centric tumors. J Hepatol. 2017; 66(2):363-73.
6. Torrecilla S, Sia D, Harrington AN, et al. Trunk mutational events present minimal intra- and inter-tumoral heterogeneity in hepatocellular carcinoma. J Hepatol. 2017; 67(6):1222-31.
7. Miao R, Luo H, Zhou H, et al. Identification of prognostic biomarkers in hepatitis B virus-related hepatocellular carcinoma and stratification by integrative multi-omics analysis. J Hepatol. 2014; 61(4):840-9.
8. Xu LX, He MH, Dai ZH, et al. Genomic and transcriptional heterogeneity of multifocal hepatocellular carcinoma. Ann Oncol. 2019; 30(6):990-7.
9. Dong LQ, Peng LH, Ma LJ, et al. Heterogeneous immunogenomic features and distinct escape mechanisms in multifocal hepatocellular carcinoma. J Hepatol. 2020; 72(5):896-908.
10. Boot GF, Haak F, Coto-Llerena M, et al. Multi-omics profiling reveals divergent biology and liver microenvironment in HCC of metastatic and de novo origin. Mol Cancer. 2026; 25(1).
11. Lu Y, Xu L, Chen W, et al. Intrahepatic Microbial Heterogeneity in Multifocal Hepatocellular Carcinoma and Its Association with Host Genomic and Transcriptomic Alterations. Cancer Discov. 2025; 15(8):1630-48.
12. Yang Y, Ni Q, Li H, et al. Genomic and the tumor microenvironment heterogeneity in multifocal hepatocellular carcinoma. Hepatology. 2025; 82(3):582-98.
13. McGranahan N, Swanton C. Clonal Heterogeneity and Tumor Evolution: Past, Present, and the Future. Cell. 2017; 168(4):613-28.
14. Hanahan D. Hallmarks of cancer-Then and now, and beyond. Cell. 2026; 189(8):2254-77.
15. Seferbekova Z, Lomakin A, Yates LR, et al. Spatial biology of cancer evolution. Nat Rev Genet. 2023; 24(5):295-313.

16. Xue R, Zhang Q, Cao Q, et al. Liver tumour immune microenvironment subtypes and neutrophil heterogeneity. Nature. 2022; 612(7938):141-7.
17. Jiang Z, Wu Y, Miao Y, et al. HCCDB v2.0: Decompose Expression Variations by Single-cell RNA-seq and Spatial Transcriptomics in HCC. Genomics Proteomics Bioinformatics. 2024; 22(1).
18. Yin J, Wang S, Liu Y. TMED2 promotes thyroid cancer tumorigenesis by being involved in mTORC1-mediated fatty acid metabolism. Biochim Biophys Acta Gen Subj. 2026; 1870(4):130910.
19. Xiao S, Jiang S, Wen C, et al. EMC2 promotes breast cancer progression and enhances sensitivity to PDK1/AKT inhibition by deubiquitinating ENO1. Int J Biol Sci. 2025; 21(6):2629-46.
20. Wu X, Liu B, Liu Y, et al. Study on the role and mechanism of TMED2 in oral squamous cell carcinoma. Int J Biol Macromol. 2025; 289(138805.
21. Dong X, Dai H, Yao L, et al. EMC2 promotes triple negative breast cancer growth by protecting FDFT1 from endoplasmic reticulum associated degradation to impair ferroptosis susceptibility. Oncogene. 2025; 44(39):3713-28.
22. Wu X, Li T, Jiang R, et al. Targeting MHC-I molecules for cancer: function, mechanism, and therapeutic prospects. Mol Cancer. 2023; 22(1):194.
23. Krenkel O, Tacke F. Liver macrophages in tissue homeostasis and disease. Nat Rev Immunol. 2017; 17(5):306-21.
24. Prakash J, Shaked Y. The Interplay between Extracellular Matrix Remodeling and Cancer Therapeutics. Cancer Discov. 2024; 14(8):1375-88.
25. Zhang Y, Song Y, Wang X, et al. An NFAT1-C3a-C3aR Positive Feedback Loop in Tumor-Associated Macrophages Promotes a Glioma Stem Cell Malignant Phenotype. Cancer Immunol Res. 2024; 12(3):363-76.
26. Medler TR, Murugan D, Horton W, et al. Complement C5a Fosters Squamous Carcinogenesis and Limits T Cell Response to Chemotherapy. Cancer Cell. 2018; 34(4):561-78 e6.
27. Wang Z, Sun C, Wang P, et al. Pan-cancer analysis of TMED2: unraveling potential immune characteristics and prognostic value in cancer therapy. Front Immunol. 2025; 16(1578627.
28. Chen J, Zhang CH, Tao T, et al. A-to-I RNA co-editing predicts clinical outcomes and is associated with immune cells infiltration in hepatocellular carcinoma. Commun Biol. 2024; 7(1):838.
29. Craig AJ, von Felden J, Garcia-Lezana T, et al. Tumour evolution in hepatocellular carcinoma. Nat Rev Gastroenterol Hepatol. 2020; 17(3):139-52.
30. Artero MR, Minery A, Nedelcev L, et al. Complement and the hallmarks of cancer. Semin Immunol. 2025; 78(101950.

31. Afshar-Kharghan V. The role of the complement system in cancer. J Clin Invest. 2017; 127(3):780-9.
32. Zhang Y, Wang X, Gu Y, et al. Complement C3 of tumor-derived extracellular vesicles promotes metastasis of RCC via recruitment of immunosuppressive myeloid cells. Proc Natl Acad Sci U S A. 2025; 122(4):e2420005122.
33. Niyonzima N, Rahman J, Kunz N, et al. Mitochondrial C5aR1 activity in macrophages controls IL-1beta production underlying sterile inflammation. Sci Immunol. 2021; 6(66):eabf2489.
34. Donne R, Lujambio A. The liver cancer immune microenvironment: Therapeutic implications for hepatocellular carcinoma. Hepatology. 2023; 77(5):1773-96.
35. Binnewies M, Roberts EW, Kersten K, et al. Understanding the tumor immune microenvironment (TIME) for effective therapy. Nat Med. 2018; 24(5):541-50.
36. Dominguez M, Dejgaard K, Fullekrug J, et al. gp25L/emp24/p24 protein family members of the cis-Golgi network bind both COP I and II coatomer. J Cell Biol. 1998; 140(4):751-65.

Supplementary Files

This is a list of supplementary files associated with this preprint. Click to download.

- Supplementaryinformation.pdf
- SupplementaryTableS1.xlsx
- SupplementaryTableS2.xlsx
- SupplementaryTableS3.xlsx
- SupplementaryTableS4.xlsx
- SupplementaryTableS5.xlsx
- SupplementaryTableS6.xlsx
- SupplementaryTableS7.xlsx